ACS APPLIED NANO MATERIALS
Cite This: ACS Appl. Nano Mater. 2019, 2, 6858−6865
Article
www.acsanm.org

Nitrogen−Sulfur-Doped Graphene Quantum Dots with Metal Ion-Resistance for Bioimaging

Zackery S. Schroer,[†] Yingfen Wu,[‡] Yuqian Xing,[‡] Xu Wu,*[,‡] Xiao Liu,[‡] Xu Wang,[†] Onnica G. Pino,[†] Chuanmin Zhou,[§] Colin Combs,[§] Qinqin Pu,[§] Min Wu,[§] Julia Xiaojun Zhao,*[,‡] and Jiao Chen*[,†]

[†]Department of Chemistry, New Mexico Highlands University, Las Vegas, New Mexico 87701, United States
[‡]Department of Chemistry, University of North Dakota, Grand Forks, North Dakota 58202, United States
[§]Department of Biomedical Sciences, The School of Medicine and Health Sciences, University of North Dakota, Grand Forks, North Dakota 58202, United States

Supporting Information

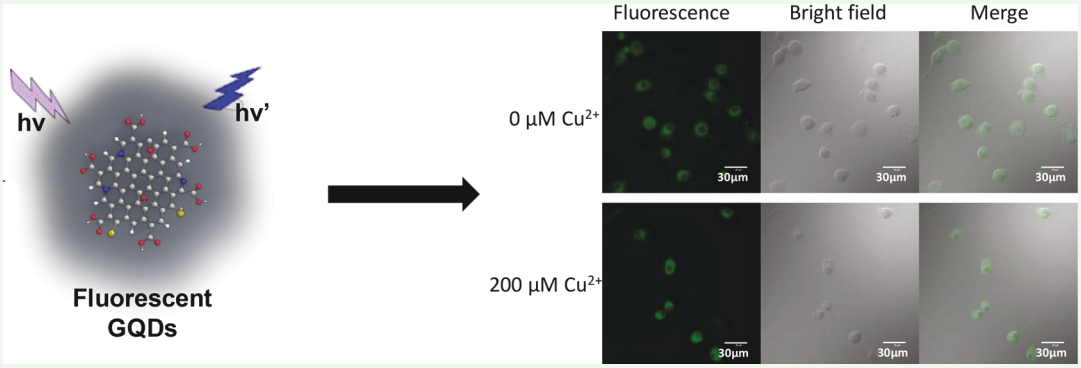

ABSTRACT: The development of ultrastable and highly fluorescent heteroatoms-doped graphene quantum dots (GQDs) for bioimaging remains a challenge due to the fluorescence quenching caused by binding between the heteroatoms-based functional groups of the GQDs and common metal ions in biological systems. Here, we developed a facile hydrothermal method to prepare nitrogen−sulfur doped GQDs (NS-GQDs). The fluorescence signals of the NS-GQDs are highly stable in the existence of different metal ions. Two natural products, aspartic acid and cysteine, were utilized as the carbon precursors and heteroatomic (nitrogen and sulfur) sources. The produced NS-GQDs showed a quantum yield up to 19.3 ± 1.7% with a maximum emission of 480 nm under the excitation of 400 nm. The elemental analysis, including X-ray photoelectron spectroscopy (XPS) and energy dispersive spectroscopy (EDS), and Fourier-transform infrared spectroscopy (FTIR), were performed to characterize the composition and surface groups of NS-GQDs. Additionally, the NS-GQDs not only showed notable photostability, but also thermostability and chemical stability. Moreover, the NS-GQDs demonstrated very low cellular cytotoxicity in vitro. Finally, the NS-GQDs were applied for fluorescence imaging of cells, which also exhibited excellent fluorescent stability even with treatment of copper ions. The results indicated that the developed novel NS-GQDs have a promising potential to be used as ultrastable fluorescent agent in the field of bioimaging and biosensing.

KEYWORDS: *graphene quantum dots, nitrogen doping, sulfur doping, bioimaging, fluorescence*

1. INTRODUCTION

Graphene quantum dots (GQDs), a zero-dimensional derivative of graphene, have emerged and ignited tremendous research interest since it was first reported in 2007. Their unparalleled properties,[1] including excellent biocompatibility, optical and electronic properties, and robust chemical inertness derived from the quantum confinement and edge effects have provided GQDs with a broad range of applications.[2−5] One of the important applications is for bioimaging in the biomedical field due to their intrinsic fluorescence properties.[4−9]

A number of methods have been developed for producing GQDs, which could be categorized into two main strategies: top-down and bottom-up methods.[10−12] The top-down methods are based on cutting larger carbon materials, such as carbon nanotubes, graphene sheets, and carbon fibers, into nanosized GQDs using physical or chemical methods.[13−17] However, the reaction conditions and purification processes of the top-down methods are complicated and time-consuming. Bottom-up methods fabricate GQDs from small molecules of carbon precursors including citric acid,[18−21] glucose,[22] amino acids,[23,24] and some natural products such as tea leaves[25] and coffee.[26] The chemical methods are usually simple and could

Received: July 10, 2019
Accepted: October 21, 2019
Published: October 21, 2019

DOI: 10.1021/acsanm.9b01309
ACS Appl. Nano Mater. 2019, 2, 6858−6865

easily manipulate the composition of the produced GQDs for desired properties. It has been reported that doping heteroatoms into GQDs could enhance their fluorescence quantum yields (QY) and tune their emission wavelengths. A few heteroatoms, B, N, S, and Si, have been introduced into GQDs using the chemical reaction methods.[27−30]

Co-doping more than two elements into GQDs have been reported, which mainly focused on codoping nitrogen and sulfur as these two elements were easily found in natural chemicals, such as amino acids. For instance, Ding et al. developed the nitrogen and sulfur codoped GQDs that exhibited strong blue emission with a QY of 54.4%. However, the fluorescence of these GQDs could be easily quenched by Fe^{3+} ion, which would cause false-negative signaling for bioimaging.[31] Recently, Chen et al. synthesized a nitrogen and sulfur codoped GQDs with excitation-independent emission behavior using pyrolysis of citric acid and cysteine.[24] By the coupling quenching abilities of silver nanoparticles with this codoped GQDs, the cyanide was monitored by the fluorescence recovery after the etching of silver nanoparticles in the presence of cyanide. Overall, the fluorescence of these NS-doped GQDs were usually easily quenched by metal ions such as Hg^{2+},[20,32,33] Cu^{2+},[34] Ag^{+},[24] etc. Although this property has been applied for sensitive detection of corresponding metal ions, the quenching has limited their applications as bioimaging agents. Therefore, the development of stable GQDs with a high QY in the existence of metal ions would be significant for bioimaging and cell tracking.

Herein, we synthesized NS-GQDs with strong fluorescence emission using a one-pot pyrolysis method. Two natural precursors, aspartic acid and cysteine, were used to introduce N, S atoms into the pristine GQDs. Doping of heteroatoms not only enhanced the quantum yield of the GQDs, but also provided extra functional groups onto the GQDs. The functional groups provide the GQDs with surface modification pathways for further applications. More interestingly, the obtained NS-GQDs showed excellent photostability regarding temperature, pH, and metal ions, which provides a promising bioimaging agent for biological samples.

2. EXPERIMENTAL SECTION

2.1. Materials. Aspartic acid, cysteine, nitric acid, hydrochloric acid, and phosphate buffered saline (PBS) tablets were obtained from Sigma-Aldrich (St. Louis, MO). The chloroauric acid was purchased from Alfa Aesar (Haverhill, MA), and the sodium citrate was from Fisher Scientific (Hampton, NH). The deionized water (18.2 MΩ·cm) was obtained from a Millipore water purification system. The murine alveolar macrophage cells (MH-S) and RAW 264.7 cells were obtained from the American Type Culture Collection (ATCC, Manassas, VA) and cultured in RPMI 1640 medium with 10% fetal bovine serum in a 5% CO_2 environment at 37 °C.

2.2. Preparation of the NS-GQDs. The NS-GQDs were prepared by pyrolyzing aspartic acid and cysteine together. Briefly, 0.15 g aspartic acid and 0.05 g cysteine were mixed together using a mortar and pestle. Then, the mixture was transferred into a glass bottle and heated up to 400 °C with a heating mantle. The color of the mixture turned to brown in 5 min, indicating the formation of NS-GQDs. Finally, 3.0 mL of distilled water was added into the solution followed by stirring for 30 min at room temperature. The resultant solution was centrifuged at 10 000 rpm for 30 min to remove the large aggregates, and the supernatant was collected and dialyzed against water (molecular weight cut-of, MWCO: 3 kDa). The final solution was stored at room temperature for further usage.

2.3. Characterization of the NS-GQDs. High-resolution transmission electron microscopy (HRTEM) and energy-dispersive X-ray spectroscopy (EDS) (Oxford, X-Max) measurements were conducted on a JEOL JEM-2100 HRTEM at an operating voltage of 200 kV. The size distribution of the NS-GQDs was obtained from the measurements of more than 500 particles in the TEM images. The UV−vis spectrum was obtained with a HP8453 UV−visible spectrophotometer. The fluorescence excitation and emission spectra were recorded using a Shimadzu RF-5301 PC spectrofluorophotometer. A Fourier-transform infrared spectrometer (FTIR) (Spectrum 400, PekinElmer) was used to collect the FTIR spectra of the NS-GQDs. The X-ray photoelectron spectrometry (XPS) measurements were conducted on an ESCALAB-MKII 250 photoelectron spectrometer (VG Co.). The Al Kα X-ray radiation was used as the X-ray source for excitation.

2.4. Fluorescence Stability of NS-GQDs at Different Temperatures, pH, and Metal Ions. An aliquot of 1.0 mL of 1.0 mg/mL NS-GQD solution was incubated in a water bath at different temperatures, ranging from 0−80 °C for 30 min. Then, the fluorescence intensity of the NS-GQD solution at different temperatures was recorded. Similarly, the pH of a solution of 1 mL, 1.0 mg/mL NS-GQD in PBS was adjusted from 2.03 to 11.86 by the addition of HCl or NaOH and followed by the fluorescence intensity measurements. In order to investigate the stability of NS-GQDs in the presence of different metal ions, 2.0 mL of 1.0 mg/mL NS-GQD solution was added with different metal ions, including Hg^{2+}, Cu^{2+}, Zn^{2+}, Fe^{3+}, Fe^{2+}, Mn^{2+}, Na^{+}, K^{+}, Ag^{+}, and Pb^{2+}. The final concentrations of the metal ions were fixed at 1.0 μM.

2.5. Solubility Investigation. In order to expand the applications of the NS-GQDs, we tested the solubility of the GQDs in different solvents. NS-GQDs solutions (1.0 mg/mL) were dispersed in different solvents, including water, CH_2Cl_2, DMSO, glycerol, THF, ethyl acetate, acetone, and EtOH before being stored for 1 month. The photos of the NS-GQDs were taken under a handy UV lamp excitation (365 nm) to check if there are any precipitants formed in different solvents.

2.6. In Vitro Fluorescence Imaging of Cells. Briefly, murine alveolar macrophage cells (MH-S) were used as model cells and cultured at 37 °C in RPMI 1640 media containing 10% fetal bovine serum in a 5% CO_2 environment overnight. Then, a 2.0 mL aliquot of 10 mg/mL NS-GQDs dispersed in the RPMI 1640 media without FBS was incubated with the MH-S cells in the plates. After 6 h of incubation, the MH-S cells were washed twice with PBS buffer to remove the free GQDs and the cells were imaged using the Zeiss LSM-510 Meta confocal fluorescence microscope. In addition, an MTT assay was conducted to investigate the cytotoxicity of the NS-GQDs on MH-S cells after incubating with different concentrations of NS-GQDs for 24 h.

2.7. Copper Ion Resistance in Cell Imaging. RAW264.7 macrophage cells were used to test the copper ion resistance of NS-GQDs in cell imaging. RAW264.7 cells were seeded in 8-well plates with the density of 10 000 cell/well overnight in RPMI 1640 media containing 10% FBS in a 5% CO_2 environment. After washing the cells with the fresh media, the media containing either NS-GQDs (1.0 mg/mL) or NS-GQDs (1.0 mg/mL) with copper ions (200 μM) were used to culture the cells for another 12 h. Then, the cells were fixed with 4% paraformaldehyde and washed with PBS three times to remove the excess NS-GQDs. The fluorescence images of these cells were taken using the Zeiss LSM-510 Meta confocal fluorescence microscope. Similarly, the cells were treated with 10.0 μg/mL semiconducting polymer dots (Pdots) as a control, which would be quenched by the copper ions.

3. RESULTS AND DISCUSSION

3.1. Design and Synthesis of the Fluorescent NS-GQDs. The objective of this work was to develop a novel method to prepare a stable and highly fluorescent GQDs through doping heteroatoms. The dopant atoms could also serve as functional groups on their surface for further modification. Thus, nitrogen and sulfur were selected as the heteroatoms for codoping into the GQDs. A number of sulfur- and nitrogen-containing molecules are potential candidates as

DOI: 10.1021/acsanm.9b01309
ACS Appl. Nano Mater. 2019, 2, 6858−6865

the precursors to fulfill this purpose. In general, an ideal precursor for the hydrothermal synthesis of GQDs should satisfy the criteria including nontoxic, inexpensive, and no surface passivation required. After a series of evaluations, aspartic acid and cysteine were chosen as precursors for the synthesis of nitrogen−sulfur doped GQDs (NS-GQDs). As shown in Scheme 1, the solid mixture of aspartic acid and cysteine was directly placed on a hot plate with the temperature set at 400 °C. The color of the heated liquid changed from colorless to pale yellow and brown eventually, suggesting the formation of NS-GQDs. The formed NS-GQDs were stable without extra surface passivation.

Scheme 1. Schematic Diagram of the Formation of NS-GQDs through the Pyrolysis of Aspartic Acid and Cysteine

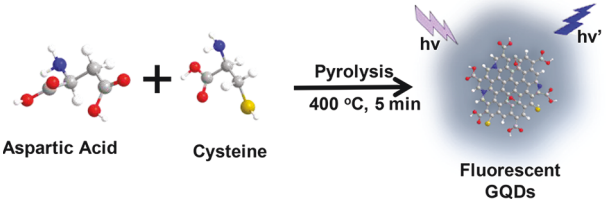

3.2. Characterization of NS-GQDs. The morphology, size, and crystal structure of the developed NS-GQDs were characterized using a HRTEM (Figure 1A−C). The lattice spacing of NS-GQDs in Figure 1B was shown as 0.286 nm, indicating a similar structure of the graphitic carbon. After measurements of more than 500 dots in TEM images, the average size of NS-GQDs was calculated to be about 3.26 ± 1.30 nm. The size distribution was shown in Figure 1C, indicating the uniform size distribution of the obtained NS-GQDs. Meanwhile, the elemental content of the NS-GQDs was analyzed using EDS (Figure 1D). The EDS results clearly showed that the NS-GQDs contained C, O, N, and S, resulting from the pyrolysis of the aspartic acid and cysteine mixture.

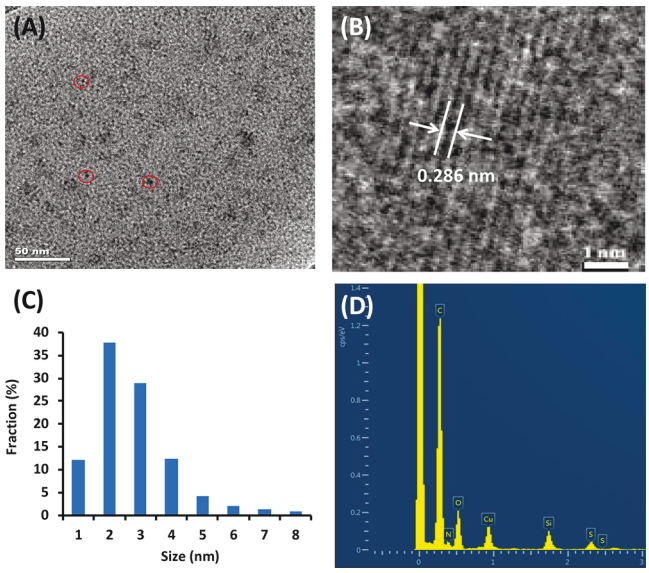

Figure 1. (A) and (B) The HRTEM images of NS-GQDs, with a lattice distance of 0.286 nm. Scale bars in A and B are 50 and 1 nm, respectively. (C) The histogram of the size distribution of NS-GQDs by measuring more than 500 particles in the HRTEM images. (D) The EDS spectrum of the NS-GQDs.

To further confirm the formation of NS-GQDs, several spectroscopic methods were used to investigate the obtained nanomaterials. First, an UV−vis absorption spectrum of the NS-GQDs was recorded (Figure 2A). Two absorption peaks at 230 and 355 nm were observed, in which the 230 nm peak indicated the $\pi-\pi^*$ transition of C═C bonds, and the 355 nm peak demonstrated the presence of the sp^2 clusters in NS-GQDs. These results were consistent with the previously reported GQDs.[17] Second, FTIR was employed to confirm the presence of different functional groups on NS-GQDs. As shown in Figure 2B, the peak at 3000 cm^{-1} indicated the presence of the C═C stretching of graphite. The presence of −OH groups was confirmed by the broad peak area at 3500 cm^{-1}. Meanwhile, the amide stretching peak around 1600 cm^{-1} and stretching vibrations of amine N−H at 3360 cm^{-1} clearly demonstrate the presence of amides and amine groups in the formed GQDs. The sharp absorption peak at 1400 cm^{-1} is due to the stretching vibration of the C−N bond. The presence of carboxyl groups was demonstrated by the peaks at ca. 1700 cm^{-1}. More importantly, the absorption peak around 1200 cm^{-1} is ascribed to the stretching vibration of a C−S bond in NS-GQDs.

Furthermore, the composition of the obtained NS-GQDs was characterized using X-ray photoelectron spectroscopy (XPS) (Figure 3). The results showed four main peaks at 284.0, 530.6, 400.0, and 160.0 eV, which were attributed to C 1s, O 1s, N 1s, and S 2p, respectively (Figure 3A). The atomic percentages of the main elements of carbon, oxygen, nitrogen, and sulfur were calculated to be about 66.9%, 18.1%, 13.1%, and 1.9%, respectively. The high-resolution XPS spectra of C 1s of NS-GQDs (Figure 3B) showed four peaks at 284.6, 285.5, 286.5, and 288. One eV, indicating the presence of C═C, C−C/C−H, C−OH, and C═N/C═O, respectively. The observation of C═C demonstrated the sp^2 carbon of graphitic structure and the other bonds suggested the sp^3 carbon in the NS-GQDs.

The N 1s spectrum (Figure 3C) showed two peaks at 399.2 and 400.5 eV due to the presence of C−N (pyrrolic N) and N−$(C)_3$(graphitic N) bands, respectively. These two peaks indicated that the sp^2 hybridized N atoms were embedded in the three sp^2 hybridized C atoms, which was in the conjugated network of graphene.

In addition, the two peaks at 163.5 and 164.9 eV in the S 2p spectra (Figure 3D) demonstrated the presence of 2p3/2 and 2p1/2 positions of the C−S bonds in NS-GQDs, respectively. These results indicated that sulfur was presented in the form of a thiophene-like structure or a thiazolidine ring in the NS-GQDs. All data from the XPS analyses suggested that nitrogen and sulfur atoms were successfully doped into the GQDs during the hydrothermal process of the mixture of aspartic acid and cysteine.

The optical properties of the developed NS-GQDs were further characterized using fluorescence spectrometry. Under the irradiation of a 365 nm UV light, the solution of the mixture of aspartic acid and cysteine showed no fluorescence (Figure 4A-a). In contrast, the solution of the NS-GQDs showed a strong blue fluorescence signal (Figure 4A-b), indicating the formation of the fluorescent NS-GQDs. Upon excitation at 360 nm, NS-GQDs showed a strong fluorescence peak at 460 nm (Figure 4B). Similar to most of the luminescent carbon nanoparticles, the fluorescence spectra of

DOI: 10.1021/acsanm.9b01309
ACS Appl. Nano Mater. 2019, 2, 6858−6865

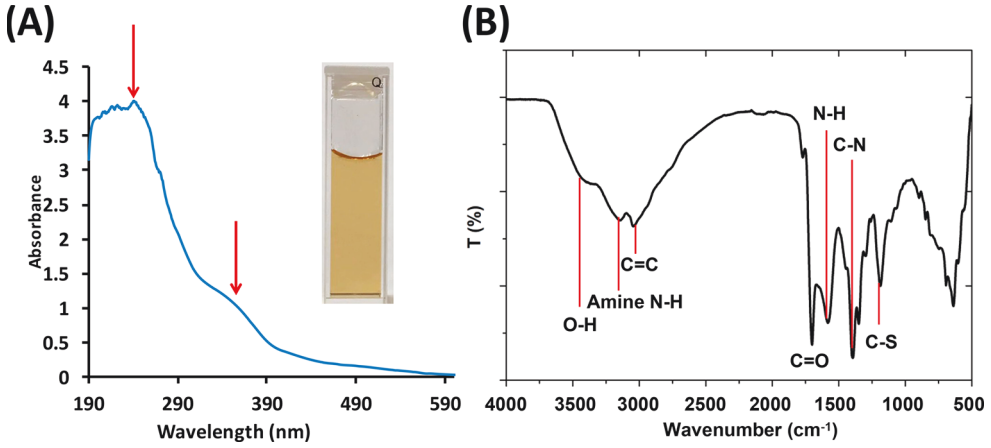

Figure 2. UV−vis absorption (A) and FTIR (B) spectra of NS-GQDs.

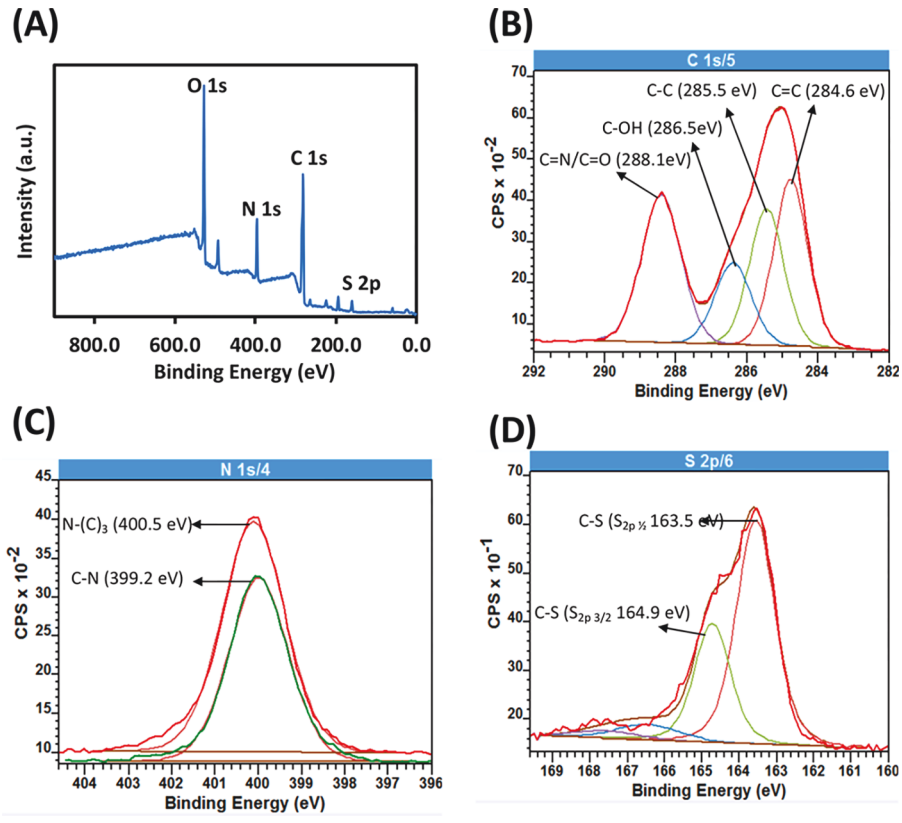

Figure 3. (A) XPS spectrum of NS-GQDs. High resolution C 1s (B); N 1s (C); and S 2p (D) spectra of NS-GQDs.

the NS-GQDs possessed an excitation-dependent manner. As the excitation wavelength increased from 340 to 520 nm, the fluorescence emission peak shifted from 440 to 550 nm (Figure 4C and D). The strongest fluorescence emission was obtained when the excitation wavelength was set to 400 nm (Figure 4C).

3.3. Photostability, Thermostability, And Chemical Stability of the NS-GQDs. In order to apply the NS-GQDs for bioimaging, especially for long-term bioimaging, the stability of the NS-GQDs, including photostability, thermostability and chemical stability, should be superior enough for this application. Therefore, we investigated the impact of these parameters on the fluorescence intensity of NS-GQDs. First, the thermal stability of the NS-GQDs was investigated as shown in Figure 5A. In the range of 0−80 °C, the fluorescence intensity of NS-GQDs showed neglectable changes at different temperatures, indicating good thermal stability of the NS-GQDs (Figure 5A). Usually, the increased temperature promotes the dynamic collision of fluorophores in the solution, resulting in the fluorescence quenching.[35] However, compared with the GQDs developed by Dr. Srivastava,[36] whose fluorescence intensity decreased by 58% when the temperature increased from 10 to 80 °C, our NS-GQDs demonstrated better thermostability. This might be caused by the possible thick surface-passivation layer of the NS-GQDs formed by the residues of the starting materials. Previous reports demonstrated that the passivation of GQDs could significantly enhance the fluorescence intensity as well as the thermal stability.[37−39]

DOI: 10.1021/acsanm.9b01309
ACS Appl. Nano Mater. 2019, 2, 6858−6865

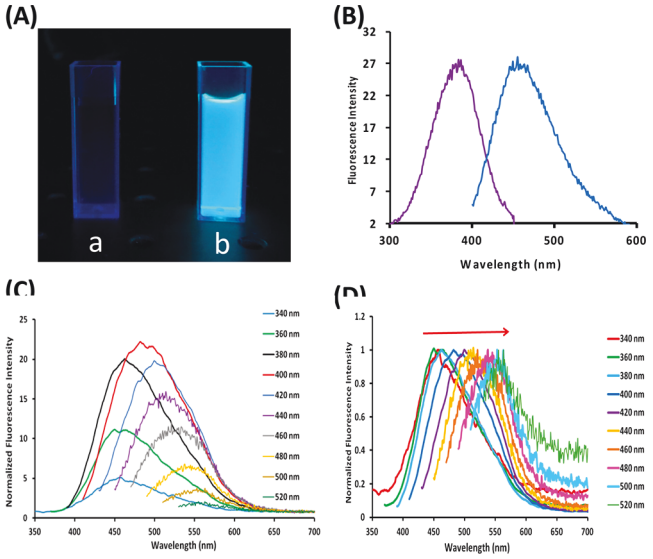

Figure 4. (A) The solution of aspartic acid and cysteine (a) and NS-GQDs (b) under the irradiation of a 365 nm UV lamp. (B) The excitation and emission spectra of NS-GQDs. λ_{ex} = 360 nm; λ_{em}: 460 nm. (C) Fluorescence emission spectra of NS-GQDs with different excitation wavelengths. (D) The normalized fluorescence spectra in C. The concentration of NS-GQDs was 1.0 mg/mL.

Though the NS-GQDs showed good thermostability, the fluorescence of the NS-GQDs is very sensitive to the pH changes. As shown in Figure 5B, when the pH increased from 2.03 to 11.86, the fluorescence intensity of NS-GQDs decreased by 64.4%. Considering that biological samples have a neutral pH around 7, we found that about 71.8% of the highest fluorescence signal remained at pH 7.16, which would still be useful for bioimaging in the physiological environment.

In this work, the most exciting phenomenon was that the fluorescence of the NS-GQDs showed extraordinary stability against metal ions. Different metal ions, commonly found in biological samples such as cells and tissues, were selected for studying the effect of metal ions on the fluorescence intensity of NS-GQDs. As shown in Figure 5C and D, 10 different metal ions, including Hg^{2+}, Cu^{2+}, Zn^{2+}, Fe^{3+}, Fe^{2+}, Mn^{2+}, Na^{+}, K^{+}, Ag^{+}, and Pb^{2+}, at a final concentration of 1.0 μM were added to the NS-GQD solution. Compared to the pure NS-GQD solution without metal ions (sample 11 in Figure 5C and the last column in Figure 5D), the fluorescence intensity of NS-GQDs kept constant while the solution remained homogeneous without aggregation or precipitation. The results demonstrated the ultrastability of the NS-GQDs against a series of metal ions. This is a very unique property of our NS-GQDs as most of the GQDs could be quenched by some kind of metal ions, such as Hg^{2+}, Fe^{3+}, and Cu^{2+}.[20,34,40] We believed that this unique metal resistance of NS-GQDs was attributed to the surface functional groups of the NS-GQDs. Usually, the fluorescence quenching of GQDs by metal ions is because the metal ions could induce the aggregation through the coordination between the surface functions groups, such as carboxyl, thiol groups, etc., and the metal ions. In the developed NS-GQDs, the surface zeta potential of −9.35 ± 0.59 mV and other surface characterization indicated that carboxyl group is absent on the surface. Therefore, the potential coordination between NS-GQDs and metal ions is

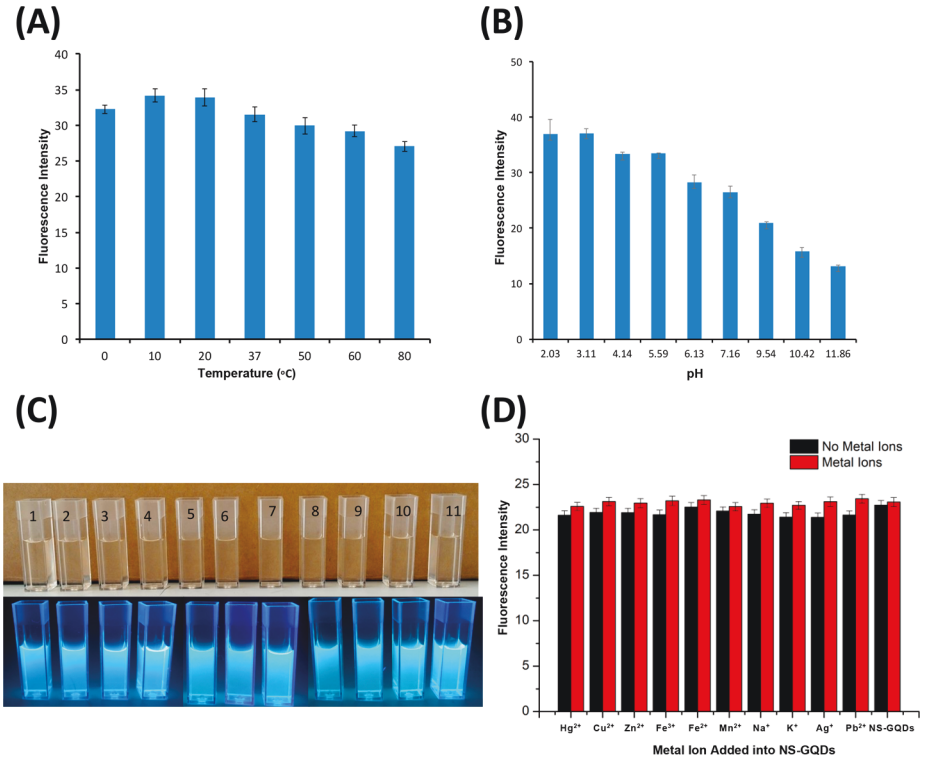

Figure 5. Effect of temperature (A), pH (B), and metal ions (C–D) on the fluorescence intensity of NS-GQDs. Items 1–10 in graph C represented the NS-GQDs with Hg^{2+}, Cu^{2+}, Zn^{2+}, Fe^{3+}, Fe^{2+}, Mn^{2+}, Na^{+}, K^{+}, Ag^{+}, and Pb^{2+}, respectively. The final concentration of metal ions was 1.0 μM. The sample 11 in graph C was the pure NS-GQDs with a concentration of 1.0 mg/mL. All solutions in C and D were in pH 7.4 at room temperature.

DOI: 10.1021/acsanm.9b01309
ACS Appl. Nano Mater. 2019, 2, 6858–6865

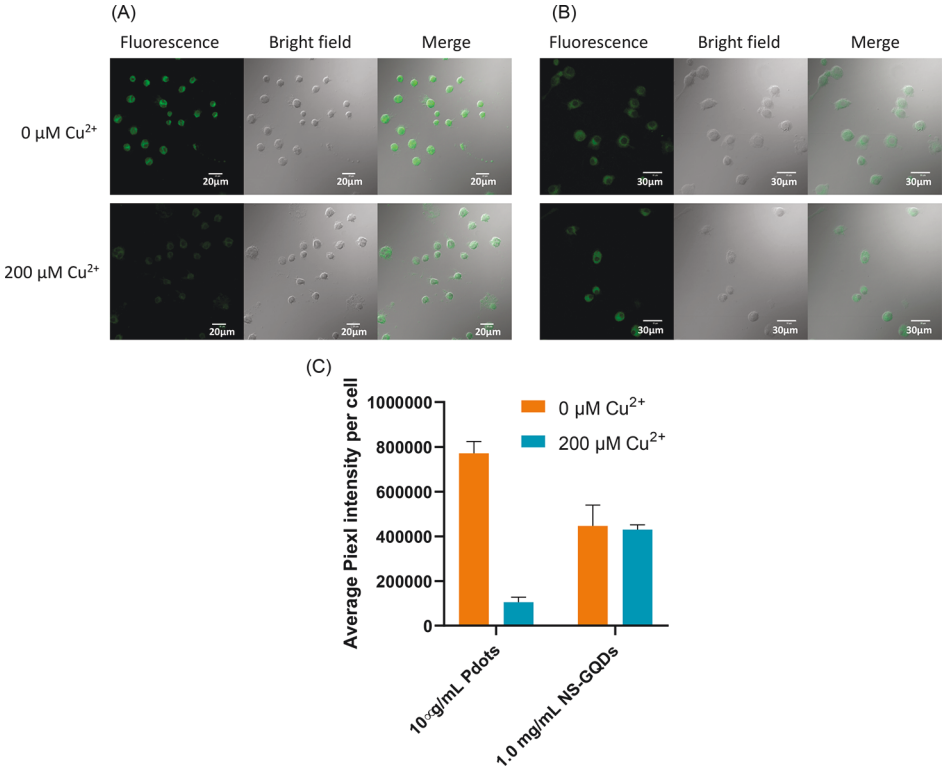

Figure 6. LSCM images of RAW 264.7 cells incubated with (A) 10.0 μg/mL Pdots, (B) 1.0 mg/mL NS-GQDs with 200 μM Cu^{2+}.

weak to induce the aggregation of the NS-GQDs, which finally showed good metal resistance.

The metal ion resistance of the NS-GQDs was further demonstrated by the comparison of the fluorescence signals of the NS-GQDs to semiconducting polymer dots (Pdots) prepared from polyfluorene (PFO). As shown in Supporting Information (SI) Figure S1, different concentrations of Cu^{2+} were incubated with these two different fluorescent nanomaterials. The fluorescence intensity of the Pdots was significantly decreased as the concentration of Cu^{2+} increased from 0 to 100 μM (Figure S1B). In contrast, the fluorescence intensity of the NS-GQDs was not affected by the different concentrations of Cu^{2+} (SI Figure S1A). These results demonstrated the excellent metal ion resistance of the prepared NS-GQDs for bioimaging.

Furthermore, the photostability of NS-GQDs was investigated using a spectrofluorometer. A NS-GQD solution was irradiated with an excitation wavelength of 400 nm for a continuous period of 30 min, the fluorescence emission at 480 nm was recorded. As shown in SI Figure S2A, a constant fluorescence signal was obtained without noticeable photobleaching. The good photostability will play a significant role for effective monitoring of various biological processes in biosensing and bioimaging.

3.4. Solubility. The developed NS-GQDs were water-soluble and therefore provided the feasibility for direct biological applications. Considering the large number of $\pi-\pi$ electrons in the structure, the NS-GQDs might possess a certain level of lipophilicity. Thus, we chose a few organic solvents to dissolve the NS-GQDs. As demonstrated in SI Figure S2B, the NS-GQDs dissolved well in DMSO, glycerol, and ethanol, which were comparable with that in water. While, its solubility was obviously reduced in other organic solvents including CH_2Cl_2, THF, ethyl acetate, and acetone. However, the partially dissolved NS-GQDs in these solvents could still emit fluorescence signals (SI Figure S2B). This amphiprotic property made the NS-GQDs very useful in both aqueous solutions and nonaqueous conditions, and thus extend their applications to a broader range of fields. The above characterizations demonstrated that the NS-GQDs could be very useful for bioimaging.

3.5. In Vitro Fluorescence Imaging. Due to the excellent fluorescence properties, we investigated the bioimaging applications of the highly fluorescent NS-GQDs in cells. After incubating MH-S cells with NS-GQDs for 6 h, the confocal images showed significant fluorescence from NS-GQDs taken up by MH-S cells through endocytosis (SI Figure S3A–C), which demonstrated that the NS-GQDs can be used for in vitro fluorescence imaging. Furthermore, the cell viability of MH-S cells was not affected by NS-GQDs up to the concentration of 1 mg/mL, as shown by the MTT assay (SI Figure S3D). The excellent biocompatibility and fluorescence imaging capacity indicated that the developed NS-GQDs could be used as a fluorescent bioimaging agent for biological samples.

In order to investigate the effect of metal ions on the bioimaging performance of the NS-GQDs in cells, we incubated the NS-GQDs with another macrophage cell line, RAW 264.7 cells, coupled with the treatment of high concentrations of copper ions. Another highly fluorescent nanoparticle, semiconducting polymer dots (Pdots),[41] was used as a control, which was quenched by the copper ions. As shown in Figure 6A, the fluorescence of Pdots in cells was significantly reduced when 200 μM Cu^{2+} was introduced, indicating the quenching effect of Cu^{2+} to Pdots in bioimaging. In contrast, in the cells stained with NS-GQDs, the treatment of 200 μM Cu^{2+} did not interfere in the fluorescence imaging capacity (Figure 6B). The results suggested that the developed

DOI: 10.1021/acsanm.9b01309
ACS Appl. Nano Mater. 2019, 2, 6858–6865

NS-GQDs had extraordinary stability against metal ions for bioimaging.

4. CONCLUSIONS

In conclusion, NS-GQDs with excellent fluorescence properties and easily functionalized groups were developed using the simple pyrolysis of the aspartic acid and cysteine. The method provided environmentally friendly, highly fluorescent NS-GQDs, which showed high photostability and thermal stability. Importantly, metal ions, such as copper, have no effect on the fluorescence of the NS-GQDs both in solution and in cell fluorescent imaging, which is different from other reported GQDs. Therefore, with further modification, the NS-GQDs have potential to act as an excellent fluorescent probe for fluorescent bioimaging.

■ ASSOCIATED CONTENT

Supporting Information

The Supporting Information is available free of charge on the ACS Publications website at DOI: 10.1021/acsanm.9b01309.

Figures S1−S3 and Table S1 (PDF)

■ AUTHOR INFORMATION

Corresponding Authors

*(X.W.) E-mail: xu.wu@und.edu.
*(J.X.Z.) E-mail: julia.zhao@und.edu.
*(J.C.) E-mail: jiao.chen@nmhu.edu.

ORCID

Xu Wu: 0000-0003-1336-9571
Julia Xiaojun Zhao: 0000-0002-9603-666X

Notes

The authors declare no competing financial interest.

■ ACKNOWLEDGMENTS

This work was supported by the U.S. National Science Foundation Grants DMR1523611(PREM) and CHE 1709160, University of North Dakota Postdoctoral Pilot Program supported by UND VPR and Art and Science College, the North Dakota Industrial Commission Grant G-041-081, and Applied Research to Address the State's Critical Needs Initiative program. Imaging studies were conducted in the UND Human and Imaging Core facility supported by NIH grant 5P20GM113123.

■ REFERENCES

(1) Bacon, M.; Bradley, S. J.; Nann, T. Graphene Quantum Dots. *Part. Part. Syst. Char.* **2014**, *31* (4), 415−428.

(2) Cao, L.; Wang, X.; Meziani, M. J.; Lu, F.; Wang, H.; Luo, P. G.; Lin, Y.; Harruff, B. A.; Veca, L. M.; Murray, D.; Xie, S.-Y.; Sun, Y.-P. Carbon Dots for Multiphoton Bioimaging. *J. Am. Chem. Soc.* **2007**, *129* (37), 11318−11319.

(3) Pan, D.; Zhang, J.; Li, Z.; Wu, M. Hydrothermal Route for Cutting Graphene Sheets into Blue-Luminescent Graphene Quantum Dots. *Adv. Mater.* **2010**, *22* (6), 734−738.

(4) Peng, J.; Gao, W.; Gupta, B. K.; Liu, Z.; Romero-Aburto, R.; Ge, L.; Song, L.; Alemany, L. B.; Zhan, X.; Gao, G.; Vithayathil, S. A.; Kaipparettu, B. A.; Marti, A. A.; Hayashi, T.; Zhu, J.-J.; Ajayan, P. M. Graphene Quantum Dots Derived from Carbon Fibers. *Nano Lett.* **2012**, *12* (2), 844−849.

(5) Schroeder, K. L.; Goreham, R. V.; Nann, T. Graphene Quantum Dots for Theranostics and Bioimaging. *Pharm. Res.* **2016**, *33* (10), 2337−2357.

(6) Gan, Z.; Xu, H.; Hao, Y. Mechanism for excitation-dependent photoluminescence from graphene quantum dots and other graphene oxide derivates: consensus, debates and challenges. *Nanoscale* **2016**, *8* (15), 7794−7807.

(7) Campbell, E.; Hasan, M. T.; Gonzalez Rodriguez, R.; Akkaraju, G. R.; Naumov, A. V., Doped graphene quantum dots for intracellular multicolor imaging and cancer detection. *ACS Biomater. Sci. Eng.* **2019** *54671*.

(8) Karimzadeh, A.; Hasanzadeh, M.; Shadjou, N.; Guardia, M. d. l. Optical Bio(sensing) Using Nitrogen Doped Graphene Quantum Dots: Recent Advances and Future Challenges. *TrAC, Trends Anal. Chem.* **2018**, *108*, 110−121.

(9) Hassan, M.; Gomes, V. G.; Dehghani, A.; Ardekani, S. M. J. N. R. Engineering carbon quantum dots for photomediated theranostics. *Nano Res.* **2018**, *11* (1), 1−41.

(10) Li, L.; Wu, G.; Yang, G.; Peng, J.; Zhao, J.; Zhu, J.-J. Focusing on Luminescent Graphene Quantum Dots: Current Status and Future Perspectives. *Nanoscale* **2013**, *5* (10), 4015−4039.

(11) Zheng, X. T.; Ananthanarayanan, A.; Luo, K. Q.; Chen, P. Glowing Graphene Quantum Dots and Carbon Dots: Properties, Syntheses, and Biological Applications. *Small* **2015**, *11* (14), 1620−1636.

(12) Paulo, S.; Palomares, E.; Martinez-Ferrero, E. Graphene and Carbon Quantum Dot-Based Materials in Photovoltaic Devices: From Synthesis to Applications. *Nanomaterials* **2016**, *6* (9), 157.

(13) Sun, M.; Ma, X.; Chen, X.; Sun, Y.; Cui, X.; Lin, Y. A Nanocomposite of Carbon Quantum Dots and TiO_2 Nanotube Arrays: Enhancing Photoelectrochemical and Photocatalytic Properties. *RSC Adv.* **2014**, *4* (3), 1120−1127.

(14) Low, C. T. J.; Walsh, F. C.; Chakrabarti, M. H.; Hashim, M. A.; Hussain, M. A. Electrochemical Approaches to the Production of Graphene Flakes and their Potential Applications. *Carbon* **2013**, *54* (Supplement C), 1−21.

(15) Zhuo, S.; Shao, M.; Lee, S.-T. Upconversion and Down-conversion Fluorescent Graphene Quantum Dots: Ultrasonic Preparation and Photocatalysis. *ACS Nano* **2012**, *6* (2), 1059−1064.

(16) Kim, J.; Suh, J. S. Size-Controllable and Low-Cost Fabrication of Graphene Quantum Dots Using Thermal Plasma Jet. *ACS Nano* **2014**, *8* (5), 4190−4196.

(17) Guo, R.; Zhou, S.; Li, Y.; Li, X.; Fan, L.; Voelcker, N. H. Rhodamine-Functionalized Graphene Quantum Dots for Detection of Fe(3+) in Cancer Stem Cells. *ACS Appl. Mater. Interfaces* **2015**, *7* (43), 23958−23966.

(18) Dong, Y.; Shao, J.; Chen, C.; Li, H.; Wang, R.; Chi, Y.; Lin, X.; Chen, G. Blue Luminescent Graphene Quantum Dots and Graphene Oxide Prepared by Tuning the Carbonization Degree of Citric Acid. *Carbon* **2012**, *50* (12), 4738−4743.

(19) Zhuang, Q.; Wang, Y.; Ni, Y. Solid-Phase Synthesis of Graphene Quantum Dots from the Food Additive Citric Acid under Microwave Irradiation and their Use in Live-Cell Imagin. *Luminescence* **2016**, *31* (3), 746−753.

(20) Anh, N. T. N.; Chowdhury, A. D.; Doong, R.-a. Highly sensitive and selective detection of mercury ions using N, S-codoped graphene quantum dots and its paper strip based sensing application in wastewater. *Sens. Actuators, B* **2017**, *252*, 1169−1178.

(21) Li, S.; Zhou, S.; Li, Y.; Li, X.; Zhu, J.; Fan, L.; Yang, S. Exceptionally High Payload of the IR780 Iodide on Folic Acid-Functionalized Graphene Quantum Dots for Targeted Photothermal Therapy. *ACS Appl. Mater. Interfaces* **2017**, *9* (27), 22332−22341.

(22) Tang, L.; Ji, R.; Cao, X.; Lin, J.; Jiang, H.; Li, X.; Teng, K. S.; Luk, C. M.; Zeng, S.; Hao, J.; Lau, S. P. Deep Ultraviolet Photoluminescence of Water-Soluble Self-Passivated Graphene Quantum Dots. *ACS Nano* **2012**, *6* (6), 5102−5110.

(23) Wu, X.; Tian, F.; Wang, W.; Chen, J.; Wu, M.; Zhao, J. X. Fabrication of Highly Fluorescent Graphene Quantum Dots Using L-Glutamic Acid for In Vitro/In Vivo Imaging and Sensing. *J. Mater. Chem. C* **2013**, *1* (31), 4676−4684.

(24) Chen, C.; Zhao, D.; Hu, T.; Sun, J.; Yang, X. Highly Fluorescent Nitrogen and Sulfur Co-Doped Graphene Quantum Dots

DOI: 10.1021/acsanm.9b01309
ACS Appl. Nano Mater. 2019, 2, 6858−6865

for an Inner Filter Effect-based Cyanide Sensor. *Sens. Actuators, B* **2017**, *241*, 779−788.
(25) Roy, P.; Periasamy, A. P.; Chuang, C.; Liou, Y.-R.; Chen, Y.-F.; Joly, J.; Liang, C.-T.; Chang, H.-T. Plant Leaf-Derived Graphene Quantum Dots and Applications for White LEDs. *New J. Chem.* **2014**, *38* (10), 4946−4951.
(26) Wang, L.; Li, W.; Wu, B.; Li, Z.; Wang, S.; Liu, Y.; Pan, D.; Wu, M. Facile synthesis of fluorescent graphene quantum dots from coffee grounds for bioimaging and sensing. *Chem. Eng. J.* **2016**, *300* (Supplement C), 75−82.
(27) Qu, D.; Zheng, M.; Du, P.; Zhou, Y.; Zhang, L.; Li, D.; Tan, H.; Zhao, Z.; Xie, Z.; Sun, Z. Highly Luminescent S, N Co-Doped Graphene Quantum Dots with Broad Visible Absorption Bands for Visible Light Photocatalysts. *Nanoscale* **2013**, *5* (24), 12272−12277.
(28) Lu, Y.-F.; Lo, S.-T.; Lin, J.-C.; Zhang, W.; Lu, J.-Y.; Liu, F.-H.; Tseng, C.-M.; Lee, Y.-H.; Liang, C.-T.; Li, L.-J. Nitrogen-Doped Graphene Sheets Grown by Chemical Vapor Deposition: Synthesis and Influence of Nitrogen Impurities on Carrier Transport. *ACS Nano* **2013**, *7* (8), 6522−6532.
(29) Yeh, T. F.; Teng, C. Y.; Chen, S. J.; Teng, H. Nitrogen-Doped Graphene Oxide Quantum Dots as Photocatalysts for Overall Water-Splitting under Visible Light Illumination. *Adv. Mater.* **2014**, *26* (20), 3297−3303.
(30) Zhang, L.; Zhang, Z. Y.; Liang, R. P.; Li, Y. H.; Qiu, J. D. Boron-Doped Graphene Quantum Dots for Selective Glucose Sensing Based on the "Abnormal" Aggregation-Induced Photoluminescence Enhancement. *Anal. Chem.* **2014**, *86* (9), 4423−4430.
(31) Ding, H.; Wei, J. S.; Xiong, H. M. Nitrogen and Sulfur Co-Doped Carbon Dots with Strong Blue Luminescence. *Nanoscale* **2014**, *6* (22), 13817−13823.
(32) Zhao, X.; Gao, J.; He, X.; Cong, L.; Zhao, H.; Li, X.; Tan, F. DNA-Modified Graphene Quantum Dots as a Sensing Platform for Detection of Hg^{2+} in Living Cells. *RSC Adv.* **2015**, *5* (49), 39587−39591.
(33) Li, L.; Wu, G.; Hong, T.; Yin, Z.; Sun, D.; Abdel-Halim, E. S.; Zhu, J.-J. Graphene Quantum Dots as Fluorescence Probes for Turn-off Sensing of Melamine in the Presence of Hg^{2+}. *ACS Appl. Mater. Interfaces* **2014**, *6* (4), 2858−2864.
(34) Wang, F.; Gu, Z.; Lei, W.; Wang, W.; Xia, X.; Hao, Q. Graphene Quantum Dots as a Fluorescent Sensing Platform for Highly Efficient Detection of Copper(II) Ions. *Sens. Actuators, B* **2014**, *190*, 516−522.
(35) Kuzkova, N.; Popenko, O.; Yakunov, A. Application of Temperature-Dependent Fluorescent Eyes to the Measurement of Millimeter Wave Absorption in Water Applied to Biomedical Experiments. *Int. J. Biomed. Imaging* **2014**, *2014*, 243564.
(36) Kumawat, M. K.; Thakur, M.; Gurung, R. B.; Srivastava, R. Graphene Quantum Dots from Mangifera indica: Application in Near-Infrared Bioimaging and Intracellular Nanothermometry. *ACS Sustainable Chem. Eng.* **2017**, *5* (2), 1382−1391.
(37) Shen, J.; Zhu, Y.; Chen, C.; Yang, X.; Li, C. Facile Preparation and Upconversion Luminescence of Graphene Quantum Dots. *Chem. Commun.* **2011**, *47* (9), 2580−2582.
(38) Shen, J.; Zhu, Y.; Yang, X.; Zong, J.; Zhang, J.; Li, C. One-Pot Hydrothermal Synthesis of Graphene Quantum Dots Surface-Passivated by Polyethylene Glycol and Their Photoelectric Conversion under Near-Infrared Light. *New J. Chem.* **2012**, *36* (1), 97−101.
(39) Hai, X.; Feng, J.; Chen, X.; Wang, J. Tuning the optical properties of graphene quantum dots for biosensing and bioimaging. *J. Mater. Chem. B* **2018**, *6* (20), 3219−3234.
(40) Li, S.; Li, Y.; Cao, J.; Zhu, J.; Fan, L.; Li, X. Sulfur-doped graphene quantum dots as a novel fluorescent probe for highly selective and sensitive detection of Fe(3+). *Anal. Chem.* **2014**, *86* (20), 10201−10207.
(41) Chan, Y. H.; Jin, Y.; Wu, C.; Chiu, D. T. Copper(II) and Iron(II) Ion Sensing with Semiconducting Polymer Dots. *Chem. Commun.* **2011**, *47* (10), 2820−2822.

DOI: 10.1021/acsanm.9b01309
ACS Appl. Nano Mater. 2019, 2, 6858−6865